

Remarkable Color Gamut Enhancement of Dye Lacquers Using Corrugated Surfaces

Sebastian Mader* and Olivier J. F. Martin

The visual appearance of any colorized object is usually determined by the spectral absorption of either pigments or dyes. One can however also colorize objects with structural colors that typically have an iridescent appearance, as seen on many beetles. The former colorization mechanism is based on the chemical absorption of the used pigments or dye, while the latter mechanism exploits optical/physical effects such as interference, diffraction, or scattering. Both mechanisms are usually engineered separately and by different specialists. Actually, they can be combined synergistically and it is shown that absorption of three different dye lacquers is significantly enhanced when applied on a corrugated metal surface. Inspired by works on emission enhancement for molecules on top of grating surfaces, these dye lacquers are applied conformally on metallic crossed gratings. We vary thickness and extinction coefficient of the dye lacquers and find that absorption can be enhanced locally by more than a factor of 20. Simulations reveal the underlying mechanisms of this enhancement and the huge color gamut that can be realized by combining otherwise colorless dye lacquers with a corrugated surface is revealed. This approach has potential for applications in sensing with focus on visual inspection like the pregnancy test.

below the wavelength of visible light and have been optimized for color generation in transmission^[17–19] as well as reflection,^[20,21] where recently polarization-tunable colors were demonstrated.^[22,23] In that case of periodic systems, the color is mainly determined by the material, periodicity, shape, and the refractive index of the surrounding medium.^[24] The color generation of plasmonic systems is based on absorption due to the excitation of surface plasmons and not on an interference-based effect, where the periodicity determines the wavelengths which can excite surface plasmons.^[14]

In this article, we generate vivid colors by strongly enhanced absorption of dye lacquers applied conformally on square crossed metallic grating surfaces with identical periodicity in both dimensions.^[25] Unlike previously published works, we focus here not only on the generation of color by the grating itself,^[20,21] but explore its possible interactions with a dye lacquer to strongly enhance the dye absorption.


Instead of the conventional approach that consists in embedding a plasmonic system in a nonabsorbing dielectric medium,^[1,20] we apply a partially absorbing dye lacquer conformally and in direct contact to the grating surface.

This idea is inspired by works of others, who measured a significant fluorescence emission enhancement for molecules placed at well-defined distances atop a metallic grating.^[26,27] This concept was also used for light extraction to improve the efficiency of a light-emitting diode.^[28] Instead of fluorescence emission, we focus here on the enhanced absorption of submicrometer thick (semi-)transparent dye lacquers applied conformally to metallic crossed gratings. Rather than varying the distance of the absorbing material to the metal surface, we vary the thickness and extinction coefficient κ of these lacquers. This detailed study reveals the mechanisms of enhancing absorption within the dye lacquer. The findings are not limited to color generation and may find applications in other fields, such as solar cell absorption improvement,^[29] Raman spectroscopy,^[30] or highly sensitive sensing applications.^[31]

1. Introduction

Producing colors with colorless metals such as silver or aluminum is a fascinating application of plasmonic systems.^[1–6] Such systems can be as simple as a single metal particle, where material, size, shape, and refractive index of the surrounding medium determine the color impression of the particle.^[7–11] Indeed, all these parameters influence the absorption amplitude and the wavelength of the localized plasmon resonance within the particle.^[12,13] On the other hand, one can also use a system supporting propagating surface plasmon-polaritons or in short surface plasmons.^[14–16] These systems are often periodic at a length scale

S. Mader, O. J. F. Martin
École Polytechnique Fédérale de Lausanne
Nanophotonics and Metrology Laboratory
EPFL-STI-IMT-NAM
ELG 238, Station 11, Lausanne CH 1015, Vaud, Switzerland
E-mail: sebastian.mader@epfl.ch

 The ORCID identification number(s) for the author(s) of this article can be found under <https://doi.org/10.1002/adpr.202100245>.

© 2021 The Authors. Advanced Photonics Research published by Wiley-VCH GmbH. This is an open access article under the terms of the Creative Commons Attribution License, which permits use, distribution and reproduction in any medium, provided the original work is properly cited.

DOI: 10.1002/adpr.202100245

2. Results and Discussion

2.1. Measurement and Simulation of Gratings Self-Color

A crossed grating is typically manufactured in photoresist by two-beam laser interference.^[32,33] The photoresist plate is exposed twice

with a standing wave pattern in the form of a linear sinusoidal grating. Rotating the plate by 90° between the two consecutive exposure steps with identical doses, a square crossed grating with a period of 300 nm in both directions is exposed in the photoresist on 6''-plates ($152.4 \times 152.4 \text{ mm}^2$).^[34] Developing the plate, transforms the exposed image in a surface relief grating, which is then copied by electroforming in nickel and grating areas of about $100 \times 100 \text{ mm}^2$ are useable for experiments as described below.^[35]

Initial experiments showed that embedding the so-formed crossed metallic grating in a dielectric medium with a refractive index n of about 1.5 changes the color in direct reflection dramatically. The color is not a result of interference-based or diffractive effects as it is the case, e.g., in gratings with periods larger than the wavelength of light. The latter gratings diffract most of the incident light to first or higher orders. As a result, the color in direct reflection consists of all incident wavelengths minus the wavelengths that are diffracted to first and higher orders.^[36] The physical mechanism behind our plasmonic system is fundamentally different as discussed below.

The insets in **Figure 1a** show that the color changes from light brown to dark brown for a positive grating profile and to violet for a negative profile upon embedding. The structure depth is identical for both grating profiles, but the color is not, which already indicates the crucial role of the profile shape. The negative profile

is a galvanic copy of the gratings initial positive profile in photoresist. Both orientations are visualized in **Figure 1b,c**, where scanning electron microscope (SEM) images of the investigated crossed gratings are shown together with a clearly asymmetric profile, emphasizing that both profiles are simple galvanically mirrored copies of each other. The chosen line colors in **Figure 1** coarsely resemble the visual appearance of the observed color and the upward pointing triangles indicate the positive orientation, while the negative orientation is marked by downward pointing ones. The microscopic images are framed with orange lines to indicate positive profile and violet lines for the negative ones. The same colors are used on the triangles for the line plots to identify them.

The gratings shape and height depend mainly on the chosen exposure dose, development time and developer type, as reported elsewhere.^[35,37] The chosen development conditions lead to a slightly nonlinear behavior and thus the grating profile cannot be described by a pure sine or cosine function. In the case of a pure sine or cosine profile, both profiles (positive and negative), would lead to identical color changes upon embedding. The color difference observed in the insets of **Figure 1a** is the result of a slight, but important asymmetry between positive and negative profiles, see **Figure 1b,c**. **Figure S1**, Supporting Information, shows a SEM image with an overlaid profile fit. The difference

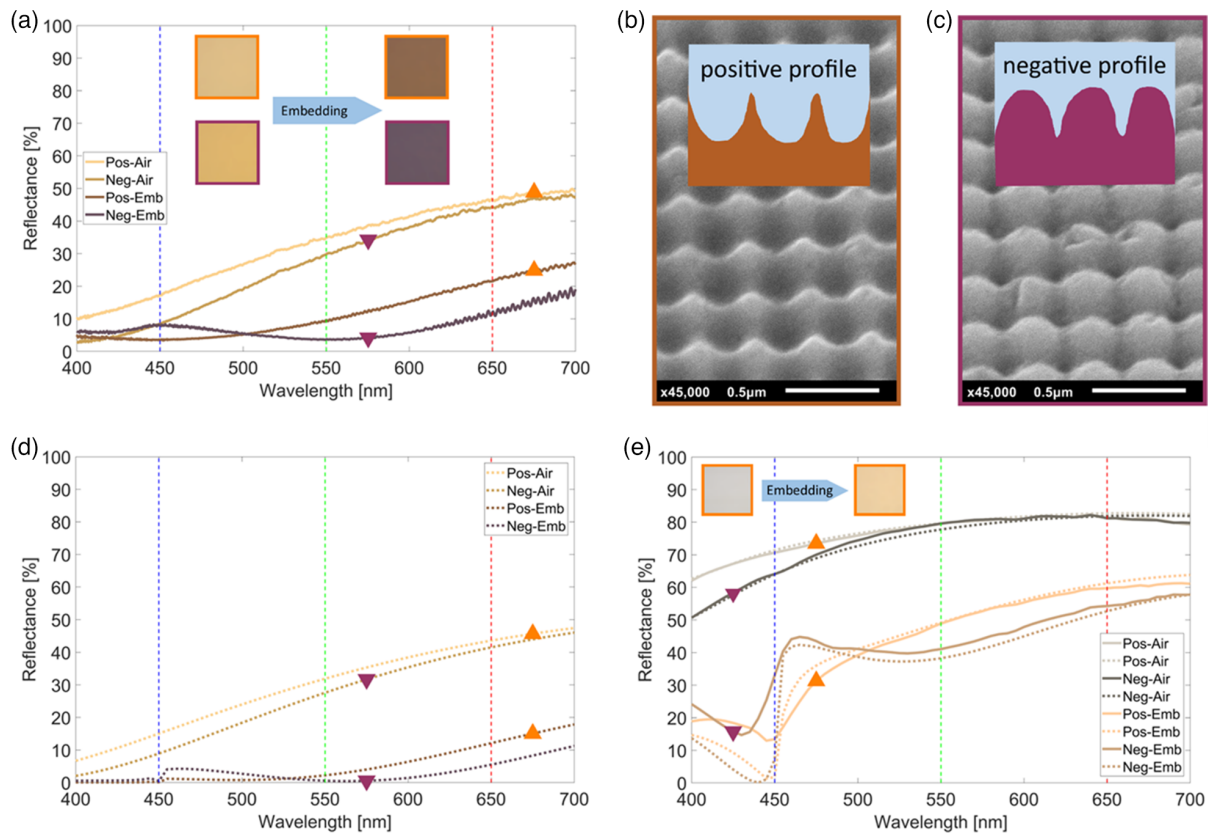


Figure 1. Experimental and simulated spectra for crossed gratings with nickel and aluminum surfaces. a) Measured reflection spectra for sinusoidal crossed gratings in nickel surrounded by air and embedded in a dielectric with refractive index $n \approx 1.5$. The optical microscope images show the color before and after embedding. b) SEM images of a crossed grating with positive profile and c) negative profile. The insets emphasize the asymmetry between the positive and negative profiles. d) Simulated spectra of the systems in (a). e) Measured (solid lines) and simulated (dotted lines) reflection spectra of the sine-like crossed gratings with aluminum surfaces.

from a pure cosine can be qualitatively depicted from Figure S2, Supporting Information and is quantified by Equation (S1), Supporting Information. The latter proves that the profile fit is indeed dominated by the cosine term and is only marginally corrected by a second- and a third-order cosine term.

Nonetheless, this minor deviation from a pure cosine renders both profiles (positive and negative) nonsymmetric, which leads to this well-visible color difference upon embedding. Larger deviations would lead to even stronger differences and gratings with identical height, but different shapes can even lead to complementary colors, see Figure S3, Supporting Information. Such nonsymmetric shapes can be achieved by modifying the development conditions or by using alternative methods such as hemispherical shell stripping.^[38] Cosine base functions up to third order rather than sine-based ones are used to enforce symmetry with respect to the center of a single grating period. The fitted profile function is then used to describe the surface in finite difference time domain (FDTD) simulations with Lumerical FDTD.^[39] Note that, a linearly polarized plane wave source impinges on the corrugated surface with a polarization angle of 45° with respect to the gratings main axes for all simulations and further details are provided in the Experimental Section. The simulated spectra in Figure 1d agree extremely well with the experimental ones reported in Figure 1a for the different studied profile orientations, both in air and embedded in a dielectric with a refractive index n of 1.5. To reach this agreement, a grating depth of 172 nm was used, which corresponds to the depth measured by atomic force microscopy (AFM), see Figure S4, Supporting Information.

Figure 1e indicates that this very good agreement between measurement and simulation also holds when the grating material is changed from nickel to aluminum. In the simulation, the semi-infinite grating material is simply changed from nickel to aluminum, while for the experimental realization, the nickel grating is overcoated with a 50 nm-thick aluminum layer. On one hand, the chosen thickness ensures that negligible light is transmitted through the aluminum layer and the nickel base grating can be excluded in simulations. On the other hand, the layer is still so thin that the profile is not significantly altered as confirmed by the good agreement in Figure 1e of the measured aluminum grating spectra with the simulated ones.

For the aluminum system, all colors are generally brighter due to the higher reflection compared to nickel, see also Figure S5, Supporting Information, for a spectral comparison of reflection by flat surfaces. The colors are also clearly different from the nickel case and so is their alteration upon embedding in a lossless dielectric: the color changes from metallic gray to a light orange, as shown in the insets of Figure 1e for the positive profile. The measured spectra in Figure 1a,e clearly indicate that the color is not based on interference effects because the characteristic regular interference minima and maxima are not present.^[40] This is also confirmed by Figure S6, Supporting Information, where the fitted profile is scaled to six depths, showing that the locations of spectral peaks and valleys are nearly constant. Contrary to the strong dependence on shape shown in Figure S4, Supporting Information, the dependence on depth is only modest as revealed by Figure S6, Supporting Information. Both investigated metals also lead to different

colors upon embedding, an effect that is not present for fully dielectric systems.^[41]

2.2. Observation of Enhanced Dye Absorption

Inspired by works on Raman spectroscopy and fluorescence emission enhancement,^[26,27,30] in an initial experiment, the grating was overcoated with a micrometer-thick yellow dye lacquer. Surprisingly, this led to an even stronger color saturation than expected by simple addition of dye and grating absorptions, probably by strongly enhancing the intrinsic dye lacquer absorption in the blue. Debating on the origin, we hypothesized that this experimentally observed effect is caused by the interaction of the grating's near field with the thick yellow dye lacquer. To prove this hypothesis that strong dye absorption in close proximity to the grating surface is responsible for this enhancement, a much thinner and red colored dye lacquer was applied by spincoating on the aluminized crossed gratings and on a plain aluminum surface for comparison. We chose a red lacquer as the grating already absorbs in the blue, see Figure 1e, to clearly investigate the origin of this effect.

Figure 2a shows the measured absorption on flat aluminum surfaces for three investigated dye lacquers with different solid contents in solution and thicknesses, as described in Table 1 in the Experimental Section. Two of these lacquers have the same concentration of dye to binder (33.3 wt%, medium concentration MC). The thinnest lacquer has a ratio of 80 wt%, high concentration (HC) and each lacquer contains at least 99% solvents to realize thicknesses smaller or equal to 50 nm. All dye lacquer layers are further encapsulated with a scotch tape of $n \approx 1.5$. The measured absorption follows the solid content concentration with thicker lacquers leading to stronger absorption. However, the dye's color is barely visible for the human eye for the thickest lacquer and not at all for the two thinner ones on plane aluminum surfaces, as confirmed by the insets in Figure 2a. The three optical microscope images are almost identical and agree with the metallic gray appearance that is observed visually. This is in great contrast to the drastic color change of the aluminized crossed grating samples shown in the inset of Figure 2b, where the color changes from a light orange to faint and then strong magenta with increasing lacquer thickness. Note that, the edge color of each microscope image corresponds to the line color of the measured reflection spectrum.

The interaction of crossed gratings and dye lacquer enhances absorption by more than 50%, compare the spectra for the coated grating samples in Figure 2b with the plain aluminum samples in Figure 2a. To model and investigate the origin of this enhanced absorption, the relative transmission of the lacquers is measured on 1 mm-thick polymethyl methacrylate (PMMA) substrates, see lower inset in Figure 2a. The relative transmission is the measured transmission of the dye lacquer coated sample divided by the transmission of a blank PMMA substrate. Based on the relative transmission, one can directly extract the approximate absorption coefficient α for the dye lacquers by Beer–Lamberts law.^[42] In a second step, the complex refractive index is retrieved by applying the Kramers–Kronig transformation to the linear-related extinction coefficient κ to obtain the modification of the real part.^[43] This direct approach has shortcomings for

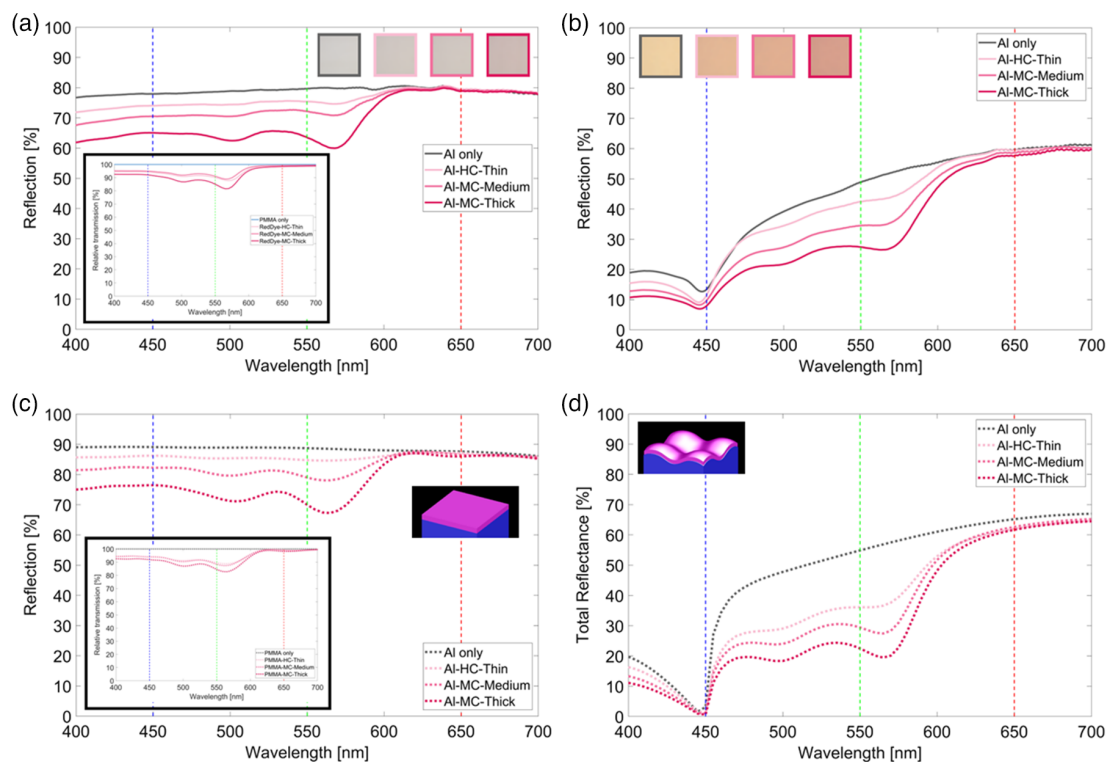


Figure 2. Three different red dye lacquers applied on plane surfaces and crossed gratings. a) Measured reflection spectra for three embedded dye lacquers coated on aluminum substrates and the bare substrate (the insets show the corresponding relative transmission dye spectra on PMMA normalized to the PMMA transmission). b) Measured reflection spectra of these systems for a positive profile crossed grating. c) Simulated spectra for the systems in panel a with the determined refractive index based on relative transmission measurements. d) Simulated spectra for the systems in panel b). The schematics in (c) and (d) illustrate the corresponding simulation geometries.

Table 1. Formulations of three experimentally investigated dye lacquers.

Lacquer	Dye content (solid lacquer) [wt%]	Solid content (solution) [wt%]	BASF orasol Red 365	Dow paraloid A11	1-Methoxy-2-propanol	Toluene
HC-Thin (13 nm)	80.0	0.25	0.20 wt% (0.150 g)	0.05 wt% (0.038 g)	49.87 wt% (37.406 g)	49.87 wt% (37.406 g)
MC-Medium (35 nm)	33.3	0.50	0.17 wt% (0.125 g)	0.33 wt% (0.250 g)	49.75 wt% (37.313 g)	49.75 wt% (37.313 g)
MC-Thick (50 nm)	33.3	1.00	0.33 wt% (0.250 g)	0.67 wt% (0.500 g)	49.50 wt% (37.125 g)	49.50 wt% (37.125 g)

thin and highly absorbing films as it fully neglects thin film effects that can significantly alter transmission as well as reflection for the highly absorbing lacquers investigated here.^[44] Consequently, we used an iterative approach to overcome these shortcomings and take these interference effects properly into account.^[44,45] The comparison of the retrieved refractive index data in Figure S7, Supporting Information, shows that the direct method overestimates extinction and thus also leads to stronger and less accurate modifications of the real part, in agreement with the prediction for slightly thicker films in the infrared.^[45] Alternatively, one could calculate the polarizability of individual dye molecules by measuring transmission of a weakly absorbing dye lacquer to avoid strong interference effects and then use the direct approach above as described in detail by Djorović et al. lately.^[43]

The iterative approach thus allows for the accurate simulation of planar systems, while the direct approach gave a reasonable

agreement (data not shown). The very good agreement between simulated and measured reflection and transmission can be confirmed by comparing the dotted lines in Figure 2c with the solid lines in Figure 2a for the same color code. The difference in absolute reflection values can be attributed to the encapsulation method as a simple scotch tape was used for all samples. Another indication are the results in Figure 2d, which also reproduce very well the trends in Figure 2b, if one compares the lines with the same color code. Furthermore, the simulations indicate that one could possibly even further enhance the absorption as they predict an even higher absorption enhancement and thus stronger color change exceeding simple addition of both individual absorptions. A possible reason for this slight discrepancy is that the lacquer is overcoated conformally to the grating surface in the simulation and the system is perfectly periodic. Both assumptions are difficult to fulfil perfectly in experiments as

the dye lacquers was applied wet, i.e., by spin coating, and the periodicity is always slightly broken due to microscopic defects and minor shape variations from the fitted profile, see Figure 1b, c and S1, Supporting Information.

2.3. Mechanisms for Absorption Enhancement

The measured direct reflection spectra in Figure 2d show a clear dip at 450 nm, with and without dye lacquers. The origin of this drop and the angular dependence of the crossed grating reflection are revealed by the dispersion diagrams^[15,46] in **Figure 3**. The dispersion diagram for the embedded grating in Figure 3a visualizes the direct reflection overlaid with three dotted lines. The dotted lines are the propagating grazing diffraction orders, i.e., those parallel to the grating surface. The yellow line corresponds to the +1st-order diffraction in x -direction, the red to +1st- and -1st-order diffraction in y -direction and the orange line to the cross terms of these orders. The grating order numbering is visualized in Figure S8, Supporting Information, and follows the definition by Palmer.^[36] The corresponding vacuum wavelengths λ_0 for these orders are often called Rayleigh wavelengths and can be calculated according to

$$\lambda_0 = n_d \cdot d / E_{\text{rel}} \quad (1)$$

where d is the 300 nm period of the crossed grating in x - and y -direction, E_{rel} is the relative energy, and n_d is the refractive index of the surrounding dielectric medium with a constant value of 1.5 here. The grating order energies are calculated in accordance with the detailed derivation of the Rayleigh wavelengths for grazing diffraction orders by Stewart and Gallaway.^[47]

The measured intensity drops at $\lambda_0 = 450$ nm in the direct reflection spectra ($k_x = 0$), see Figure 2b, coincides with a drop in the simulated spectra in Figure 3a ($E_{\text{rel}} = 1$, $\lambda_d = \lambda_0/n = 300$ nm). This is also the starting point of the yellow 1st-order diffraction curve. Every energy below this curve supports no propagating diffraction orders and has a generally high direct reflection. The dispersion diagram might be divided into four regions and the yellow line also marks the upper bound of region

I of this division. Region II is surrounded by all three dotted lines and has intermediate reflection values. Region III is spanned by the orange and red dotted line and the reflection is only about a third of the highly reflecting region I. The lowest reflection values are found in the dark region IV above the red dotted line.

This dark region IV might be neglected for the color generation as most light here is either absorbed or redirected to propagating diffraction orders. The three dotted lines thus mark energy levels at which the direct reflection significantly changes. The drastic changes in reflection can thus be attributed to appearing and disappearing diffraction orders.^[47] This also holds for crossed gratings overcoated with a thick dye lacquer, as shown in Figure 3b. The dye has a minor impact on the bright region I except for small values of k_x , but reduces noticeably the reflection in regions II and III, while the dark region IV is only slightly darker. The two absorption peaks of the dye lacquer at $\lambda_{0,1} = 500$ nm ($E_{\text{rel}} = 0.9$) and $\lambda_{0,2} = 565$ nm ($E_{\text{rel}} = 0.8$) are also prominent in the dispersion diagram. The solid and dashed pink line mark these absorption peaks, which are independent of the incident angle as expected. The avoided crossing between the dye absorption bands and the 1st diffraction order is clearly visible in Figure 3b, especially for $\lambda_{0,2} = 565$ nm ($E_{\text{rel}} = 0.8$). By changing the grating period or the absorption peak wavelength of the dye lacquer, one can thus easily alter the reflection. The latter is explored in the following.

First, let us however investigate why the dye lacquer absorption on top of an aluminum crossed grating can be enhanced significantly compared with applying the same lacquer on top of flat surfaces, as indicated by Figure 2c,d. The origin of this absorption enhancement is attributed to the local field enhancement, which is already noticeably stronger for a flat aluminum surface compared with a flat PMMA surface due to high reflection at the aluminum interface, compare intensity distributions in **Figure 4a,b**.

All results in Figure 4 are based on systems embedded in a dielectric medium and the dye lacquer is 50 nm thick, wherever it is applied. The simulations are evaluated at $\lambda_0 = 500$ nm, where the complex refractive index of the dye lacquer is about $1.52 + 0.10i$, which differs only marginally from the constant dielectric embedding material and PMMA index of 1.5. Consequently, the standing wave pattern maximum intensity

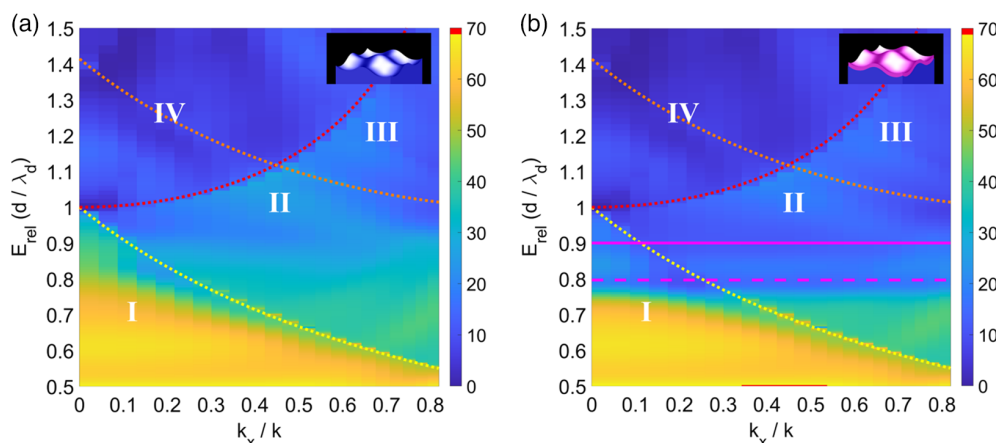


Figure 3. Simulated dispersion diagrams based on the direct reflection for embedded aluminum crossed gratings with a positive profile. a) Without and b) with a 50-nm thick conformal dye lacquer atop the grating surface. The color maps show the direct reflection of the systems and the insets the simulation geometry.

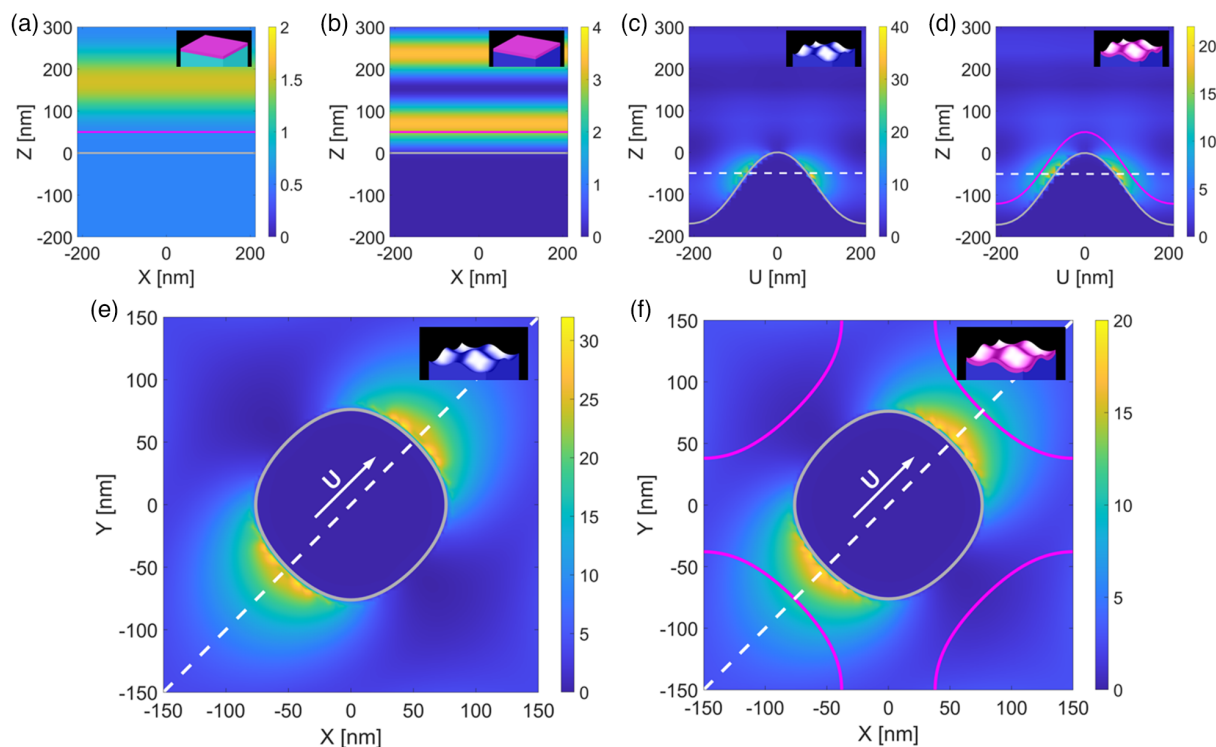


Figure 4. Simulated intensity distributions at $\lambda_0 = 500$ nm. a) PMMA substrate overcoated with a 50 nm-thick dye lacquer. b) Overcoated aluminum substrate. Positive profile crossed grating c) without and d) with conformal dye lacquer overcoating. e, f) xy crosscuts for the corresponding crossed gratings at the locations marked by the dashed white lines in panels (c, d). The insets in each panel show the corresponding simulation geometries.

for the PMMA system within the whole simulation region is smaller than 1.54 and smaller than 0.59 at the top of the dye lacquer and relatively constant within the 50 nm-thick dye lacquer. On the contrary, the maximum intensity above a flat aluminum surface is smaller than 3.74 within the whole simulation region and around 2.92 at the top interface of the dye lacquer and 0.21 at the bottom. The maximum possible intensity for such a two-beam interference is four,^[37] but the slightly lower value of 3.74 observed here results from the “only” 93.5% light reflection at $\lambda_0 = 500$ nm for the aluminum surface. On average, the intensity is about 1.51 within the dye lacquer and thus more than twice larger compared with the case of the dye lacquer above the PMMA surface. The formed standing wave pattern atop the aluminum surface, clearly visible in Figure 4b, is thus the main reason for the about twice higher absorption within the dye lacquer above aluminum compared with PMMA with a rather modest homogenous intensity distribution, see Figure 4a.

The field enhancement caused by the crossed grating is even larger. The mean intensity for the 1% highest intensity values within the whole simulation area is 25.4 for the embedded grating in Figure 4c and 16.3 for the grating overcoated with a 50 nm-thick dye lacquer, see Figure 4d. The peak values can be extracted from the corresponding color bars, which are the rounded-up integer values of the maximum intensity value. In the case of an embedded grating, the peak and mean intensity values exceed the theoretical maximum value of four for two-beam interference by more than a factor of 6.^[37] This strong field enhancement is due to the standing wave patterns resulting from grazed propagating and evanescent grating orders.^[48,49]

The magenta-colored solid line in Figure 4d marks the top surface of the dye lacquer, while the gray-colored solid lines in Figure 4a–d mark the top surfaces of aluminum or PMMA, respectively. These lines are also plotted in Figure S9, Supporting Information, which rescales Figure 4 to a maximum value of four (maximum enhancement atop a plane surface). The rescaled plot shows that the exceptional high intensity region exceeds the lacquer, and one could exploit this with slightly thicker dye lacquers. The logarithmically scaled plot of the intensity distributions in Figure S10, Supporting Information, highlights that the enhancement resembles a dipolar emission pattern. The white dashed lines at $z = -50$ nm in Figure 4c, d are the locations of the xy crosscuts shown in Figure 4e, f. Both patterns clearly show that the field enhancement is along the polarization of the incident light, the u -direction. Note that, the crosscuts in Figure 4c, d were taken along the u -direction marked by the diagonal white dashed lines in Figure 4e, f.

2.4. Demonstration of Color Gamut Enhancement

The previous results demonstrate that applying a dye lacquer on top of a crossed grating, leads to a strong absorption enhancement within the dye lacquer compared with the same lacquer on top of a plane aluminum interface. On one hand, this potentially enables one to apply less dye for the same absorption and associated color appearance. On the other hand, it also provides a mean to greatly tune the color appearance of the system in direct reflection by modifying the dyes absorption band as will be outlined below.

To study this effect with simulations, we create five artificial dye lacquers with corresponding complex refractive indices, see Figure S11, Supporting Information. Their absorption peaks are located at chosen central wavelengths λ_c that span from 450 to 650 nm in 50 nm steps and have a Gaussian shaped absorption profile with a full width half maximum of 33.3 nm. The chosen simple absorption shape is very easy to depict visually in all the results below. The maximum extinction coefficient κ (imaginary part of the complex refractive index) is kept constant at 0.2, while the thickness of the dye lacquer is varied for each central wavelength λ_c with its associated color. This ensures that when light passes the lacquer once, the transmitted intensity I is constant at λ_c for all layers according to the Beer–Lambert law

$$I = I_0 \exp(-\alpha d_c) = I_0 \exp(-4\pi\kappa d_c / \lambda_0) \quad (2)$$

where I_0 denotes the incident intensity, α the absorption coefficient, κ the imaginary part of the dye lacquers refractive index, λ_0 the vacuum wavelength, and d_c the color-dependent thickness of the dye lacquer.^[42,50] To keep the transmitted intensity value constant for all five dye lacquers, d_c is varied according to

$$d_c = d_{550} \lambda_c / 550 \text{ nm} \quad (3)$$

where d_{550} is the thickness of 50 nm for the green absorbing dye lacquer at $\lambda_0 = 550$ nm. Blue absorbing dye lacquers will thus be thinner and red absorbing ones thicker. This variation leads to nearly constant absorption for all five dye lacquers applied on top of aluminum or PMMA substrates, as confirmed by Figure 5a. This is in contrast to the results in Figure 2a,c as the absorption band in the present calculations is narrower and the lacquer thickness is adapted to the peak absorption at λ_c for each band. This effectively balances out by design the standing wave enhancement due the reflected light at the aluminum interface for all five lacquers.^[44]

Applying the lacquer conformally on top of a positive profile crossed grating leads again to a strongly enhanced absorption of the dye lacquer, compare Figure 5a,b. This enhancement by the grating is nearly independent of wavelength, which is somewhat unexpected. It is attributed again to strong near field enhancement caused by propagating grazing and evanescent grating orders. It is very remarkable that the grating supports nearly constant enhancement across the entire visible spectrum (VIS). Based on the simulated spectra, we calculated the color coordinates for a chromaticity diagram for a D65 light source (CIE 1964).^[51]

The calculated coordinates are marked by colored circle in Figure 5c–e that match the colors used for the spectra in Figure 5a. Additionally, the location of an uncoated aluminum

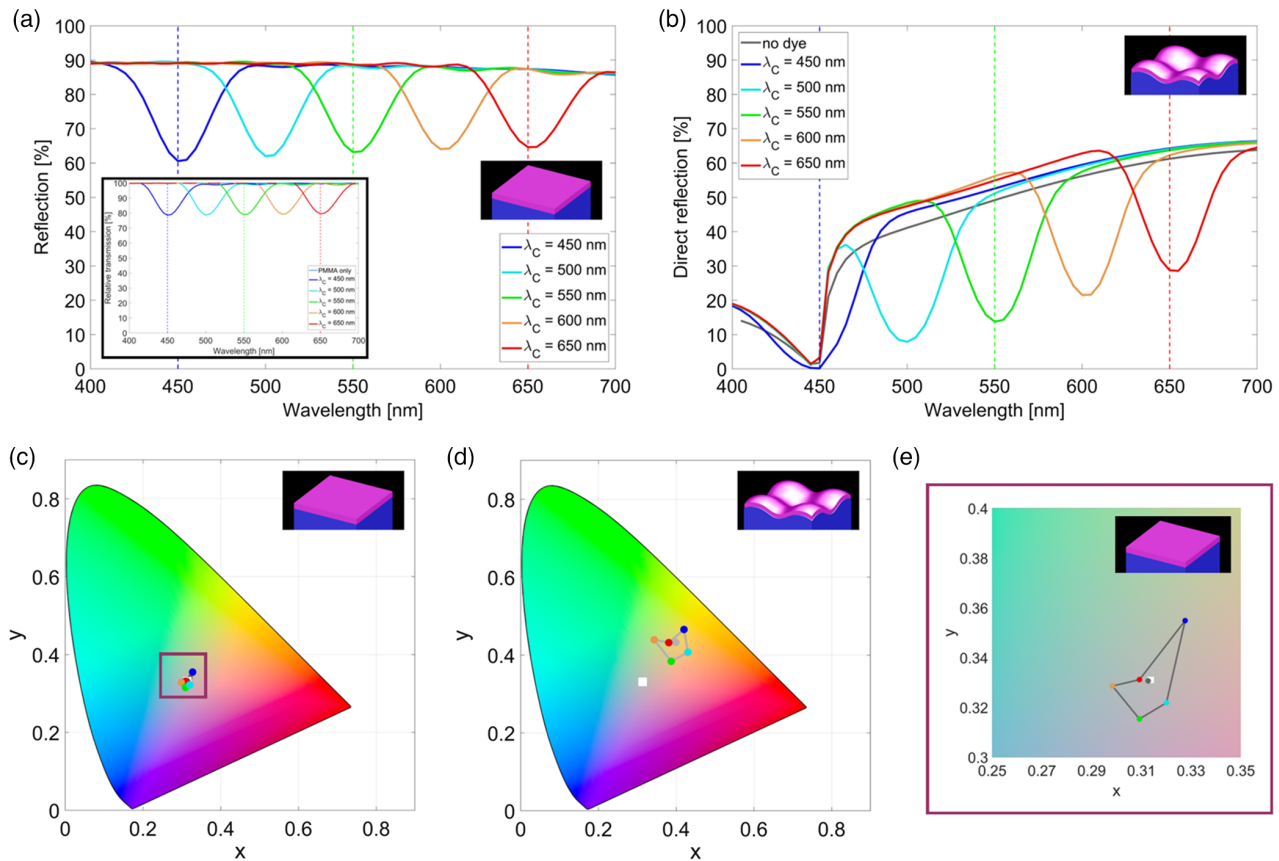


Figure 5. Simulated response of five different dye lacquers applied conformally on plane surfaces and crossed gratings. a) Simulated reflection spectra for five embedded dye lacquers coated on aluminum substrates (the inset shows the corresponding relative transmission dye spectra on PMMA normalized to PMMA transmission). b) Simulated reflection spectra for a positive profile crossed grating conformally overcoated with these lacquers. c) Chromaticity diagram for the systems in panel a). d) Chromaticity diagram for the systems in (b). e) Enlarged part of (c) to clearly visualize the area spanned by the five dye lacquers around the white point. The insets on the right of each panel show a schematic visualization of the modelled systems.

mirror is added to the diagram as a gray circle in Figure 5c, which is close to the white point resulting from the nearly uniform reflectivity across the visible spectrum, see Figure 5a. The chromaticity diagram for the plane aluminum system reveals that, albeit the clearly visible absorption in Figure 5a, the produced colors are all located at or very close to the white point, which is marked by a white square. The gray lines connecting the colored disks span a very small area that should be accessible by mixing the dye lacquers. The points are so close that only the enlarged part of the diagram in Figure 5e clearly reveals the location of each dye.

Comparing the chromaticity diagrams in Figure 5c,d confirms that the crossed grating widens the possible color gamut. The resulting color area is more than five times larger compared with the one obtained for a flat aluminum substrate, confirming the strong color enhancement possibilities of the system. This comes at the cost that the resulting colors are not anymore centered around the white point, but somewhere around a light orange, corresponding to the grating color impression without lacquer, marked also by a gray circle in Figure 5d.

This color gamut can be increased even further by applying artificial dye lacquers with three times larger FWHM and double thickness, see Figure S12, Supporting Information. The maximum extinction coefficient κ (imaginary part of the complex refractive index) is again kept constant at 0.2, see Figure S13, Supporting Information. One can realize with this broader absorbing dye lacquers atop the grating all colors except blue, because of the grating's light orange self-color (gray dot). This orange color is mainly a result of the very low reflection below its resonant reflection minimum at 450 nm. The wavelength of the minimum is solely determined by the grating period, see Figure S14, Supporting Information, while the minimum reflection value depends on shape and depth, see Figure S3 and S6, Supporting Information, respectively.

Consequently, a shorter pitched grating with its resonant absorption in the ultraviolet (UV) rather than in the blue at 450 nm could indeed be used to realize all colors. Initial simulations based on a grating with a 210 nm instead of a 300 nm period show that it is indeed possible to create a large color gamut around the white point, see Figure S15, Supporting Information.

3. Conclusion

Baffled by an observed color change upon embedding of a corrugated surface in the form of a crossed grating, we have investigated the origin of wavelength-dependent absorption and showed that material, shape, and dielectric environment of the corrugation determine the resulting gratings color. Inspired by works on fluorescence emission enhancement, we found that the dye absorption within an almost colorless appearing dye lacquers can be significantly altered and enhanced by its interaction with a grating. The enhancement of the dye lacquers intrinsic absorption was attributed to strong local field enhancement caused by evanescent and grazing propagating diffraction orders. For a set of artificial dye lacquers, it was even shown how the achievable color gamut of these lacquers can be significantly enhanced when they are conformally coated as a very thin layer (<100 nm) on top of a corrugated surface.

We believe that these findings will find application in biosensing,^[52] especially for those relying on visual inspection like the pregnancy test. The methodology allows for applying minute amounts of an almost colorless substance on top of the corrugated surface to create a drastic and clearly visible color change.^[53,54] The fact that very thin layers of these substances are sufficient makes the principle especially promising for any application that relies on diffusion of, e.g., a gas into the layer to produce absorption due to minimal diffusion times.^[55,56] Applications could include fast gas sensors and PH detectors. The submicrometer thickness also minimizes the amount of any substance needed for detection and so scarce, difficult to produce or extremely expensive substances can be employed for sensing, i.e., for Raman spectroscopy.^[38]

Besides sensing, we can also envision applications in document authenticity protection. The lithographic combination of mirror and grating elements or the combination/rasterization of different crossed gratings with the same dye lacquer can be used for printing with submicrometer resolution. The dyes absorption will be enhanced locally depending on the corrugated or flat surface beneath it.

4. Experimental Section

Aluminum Evaporation: The aluminum layer was evaporated with a Leybold Heraeus L560 by electron-beam evaporation. For the deposition, the chamber was evacuated to a pressure of 4.6×10^{-5} mbar, and the deposition rate was adjusted to 0.4–0.6 nm s⁻¹.

Simulation Setup: All simulations were performed with Lumerical FDTD,^[39] where a linearly polarized broadband source from $\lambda = 300$ to 800 nm was used to illuminate the crossed gratings. The simulation region was set to $300 \times 300 \times 2000$ nm³ with a conformal meshing of variant 1 with an accuracy of 7. The mesh size was overwritten in the region, where the grating and dye are located to a maximum size of $3 \times 3 \times 1.5$ nm³ to avoid significant staircasing effects of the gratings profile. Bloch-type periodic boundary conditions were selected laterally and perfect matching layers with 32 layers in z-direction. Power and grating-order detectors were placed at appropriate positions in accordance with the recommendations by Lumerical to achieve the highest possible accuracy in reflection and grating order power detection. The material data of nickel and aluminum were based on literature values by Palik.^[57]

Dye Lacquer Formulation and Coating: The dye lacquers consisted of four commercially available components, mainly two solvents as the solid content of each lacquer was less or equal to 1%. We added 1-methoxy-2-propanol to toluene, stirred, and heated the mixture to 60 °C. We combined it with the binder Dow Paraloid A11 while stirring and stirred for 30 min before cooling to room temperature, when the dye BASF Orasol Red 365 was amended and stirred for another 5 min to create a homogenous and fully mixed solution. The solutions were applied on the gratings by spincoating at 3000 rpm for 30 s, after which they were dried for 15 min in a convection oven at 75 °C to form the solid lacquer. This results in three different dye lacquer thicknesses were 13 nm (thin), 35 nm (medium), and 50 nm (thick), respectively. The recipes for 75 g of each lacquer are summarized in Table 1. Note that, the ratio of binder and dye of the medium concentrated dye lacquers was constant.

Spectral Measurements: All direct reflection measurements were carried out with a self-build spectroscopic setup. The light of a broadband light source Thorlabs SLS201/M was guided and collimated with the bifurcated reflection probe Avantes FCR-7UVIR200-2-ME resulting in a measurement spot diameter of about 2.5 mm. The collimated light beam hit the sample at a distance of about 50 mm, and the reflected part was guided again by the bifurcated reflection probe to the Avantes Avatec ULS3648-USB2 spectrometer. Thus, illumination and collections angle

were about 1.4°. A broadband dielectric mirror Thorlabs BB1-E02 was used as a reference for all measurements.

Supporting Information

Supporting Information is available from the Wiley Online Library or from the author.

Acknowledgements

The authors gratefully acknowledge the assistance of Thomas Mayerhöfer for valuable discussions and providing us with high accuracy refractive index data of the investigated lacquers using his iterative approach.

Conflict of Interest

The authors declare no conflict of interest.

Authors Contributions

S.M. conceived the idea, performed experiments and simulations. Both authors analyzed and discussed the results and co-wrote the manuscript.

Data Availability Statement

Research data are not shared.

Keywords

coatings, gratings, light–matter interactions, plasmonics, subwavelength materials

Received: August 19, 2021

Revised: October 26, 2021

Published online: December 21, 2021

- [1] A. Kristensen, J. K. W. Yang, S. I. Bozhevolnyi, S. Link, P. Nordlander, N. J. Halas, N. A. Mortensen, *Nat. Rev. Mater.* **2016**, 2, 16088.
- [2] X. Zhu, C. Vannahme, E. Højlund-Nielsen, N. A. Mortensen, A. Kristensen, *Nat. Nanotechnol.* **2016**, 11, 325.
- [3] J.-M. Guay, A. C. Lesina, G. Côté, M. Charron, D. Poitras, L. Ramunno, P. Berini, A. Weck, *Nat. Commun.* **2017**, 8, 1.
- [4] M. K. Hedayati, M. Elbahri, *Plasmonics* **2017**, 12, 1463.
- [5] F. Mao, A. Davis, Q. C. Tong, M. H. Luong, C. T. Nguyen, I. Ledoux-Rak, N. D. Lai, *Plasmonics* **2018**, 13, 2285.
- [6] M. Song, D. Wang, S. Peana, S. Choudhury, P. Nyga, Z. A. Kudyshev, H. Yu, A. Boltasseva, V. M. Shalaev, A. V. Kildishev, *Appl. Phys. Rev.* **2019**, 6, 041308.
- [7] J. P. Kottmann, O. J. F. Martin, D. R. Smith, S. Schultz, *Opt. Express* **2000**, 6, 213.
- [8] Y. Sun, Y. Xia, *Analyst* **2003**, 128, 686.
- [9] W. A. Murray, W. L. Barnes, *Adv. Mater.* **2007**, 19, 3771.
- [10] J. M. McMahon, G. C. Schatz, S. K. Gray, *Phys. Chem. Chem. Phys.* **2013**, 15, 5415.
- [11] S. Mader, O. J. F. Martin, *Opt. Express* **2018**, 26, 27089.
- [12] S. Maier, *Plasmonics: Fundamentals and Applications*, Springer US, Boston, MA **2007**.
- [13] W. Zhang, O. J. F. Martin, *ACS Photonics* **2015**, 2, 144.
- [14] H. Raether, *Surface Plasmons on Smooth and Rough Surfaces and on Gratings*, Springer-Verlag, Berlin Heidelberg, Germany **1988**.
- [15] A. V. Zayats, I. I. Smolyaninov, *J. Opt. A: Pure Appl. Opt.* **2003**, 5, S16.
- [16] L. Novotny, B. Hecht, *Principles of Nano-Optics*, Cambridge University Press, Cambridge, MA **2012**.
- [17] H.-S. Lee, Y.-T. Yoon, S.-S. Lee, S.-H. Kim, K.-D. Lee, *Opt. Express* **2007**, 15, 15457.
- [18] Q. Chen, D. R. S. Cumming, *Opt. Express* **2010**, 18, 14056.
- [19] I. Koirala, V. R. Shrestha, C.-S. Park, S.-S. Lee, D.-Y. Choi, *Sci. Rep.* **2017**, 7, 40073.
- [20] J. S. Clausen, E. Højlund-Nielsen, A. B. Christiansen, S. Yazdi, M. Grajower, H. Taha, U. Levy, A. Kristensen, N. A. Mortensen, *Nano Lett.* **2014**, 14, 4499.
- [21] S. Wu Sr., Y. Ye, L. Chen, in *Plasmonics III*, International Society for Optics and Photonics, Bellingham, WA **2018**, p. 1082418.
- [22] M. Song, X. Li, M. Pu, Y. Guo, K. Liu, H. Yu, X. Ma, X. Luo, *Nanophotonics* **2018**, 7, 323.
- [23] M. Song, D. Wang, Z. A. Kudyshev, Y. Xuan, Z. Wang, A. Boltasseva, V. M. Shalaev, A. V. Kildishev, *Laser Photonics Rev.* **2021**, 15, 2000343.
- [24] P. Feng, W.-D. Li, W. Zhang, *Opt. Express* **2015**, 23, 2328.
- [25] S. Kinoshita, S. Yoshioka, J. Miyazaki, *Rep. Prog. Phys.* **2008**, 71, 076401.
- [26] K. G. Sullivan, O. King, C. Sigg, D. G. Hall, *Appl. Opt.* **1994**, 33, 2447.
- [27] P. Andrew, W. L. Barnes, *Phys. Rev. B* **2001**, 64, 125405.
- [28] J. M. Lupton, B. J. Matterson, I. D. W. Samuel, M. J. Jory, W. L. Barnes, *Appl. Phys. Lett.* **2000**, 77, 3340.
- [29] A. Williamson, É. McClean, D. Leipold, D. Zerulla, E. Runge, *Appl. Phys. Lett.* **2011**, 99, 093307.
- [30] W. Knoll, M. R. Philpott, J. D. Swalen, A. Girlando, *J. Chem. Phys.* **1982**, 77, 2254.
- [31] G. Ruffato, G. Zacco, F. Romanato, in *Plasmonics—Principles and Applications*, IntechOpen, London **2012**, pp. 419–444.
- [32] M. L. Schattenburg, E. H. Anderson, H. I. Smith, *Phys. Scr.* **1990**, 41, 13.
- [33] A. A. Ushkov, I. Verrier, T. Kampfe, Y. Jourlin, *Opt. Express* **2020**, 28, 16453.
- [34] S. C. Kitson, W. L. Barnes, J. R. Sambles, *IEEE Photonics Technol. Lett.* **1996**, 8, 1662.
- [35] B. Bläsi, *Holographisch hergestellte Antireflexoberflächen für solare und visuelle Anwendungen, Dissertation, University of Freiburg*, **2000**.
- [36] C. Palmer, *Diffraction Grating Handbook*, MKS Instruments, Rochester **2020**.
- [37] B. de A. Mello, I. F. da Costa, C. R. A. Lima, L. Cescato, *Appl. Opt.* **1995**, 34, 597.
- [38] P. Krohne-Nielsen, S. M. Novikov, J. Beer mann, P. Morgen, S. I. Bozhevolnyi, O. Albrektsen, *J. Raman Spectrosc.* **2012**, 43, 834.
- [39] Lumerical Inc., *FDTD Solutions R2017a*, **2020** <https://www.lumerical.com/products/fdtd/>.
- [40] R. Ameling, H. Giessen, *Laser Photonics Rev.* **2013**, 7, 141.
- [41] R. L. Renesse, *Optical Document Security*, Artech House, London **2005**.
- [42] T. G. Mayerhöfer, S. Pahlow, J. Popp, *ChemPhysChem* **2020**, 21, 2029.
- [43] A. Djorović, M. Meyer, B. L. Darby, E. C. Le Ru, *ACS Omega* **2017**, 2, 1804.
- [44] T. G. Mayerhöfer, S. Pahlow, U. Hübner, J. Popp, *Analyst* **2020**, 145, 3385.
- [45] T. G. Mayerhöfer, S. Pahlow, U. Hübner, J. Popp, *Anal. Chem.* **2020**, 92, 9024.

- [46] T. Ochiai, K. Sakoda, *Phys. Rev. B* **2001**, 63, 125107.
- [47] J. E. Stewart, W. S. Gallaway, *Appl. Opt.* **1962**, 1, 421.
- [48] W. L. Barnes, T. W. Preist, S. C. Kitson, J. R. Sambles, *Phys. Rev. B* **1996**, 54, 6227.
- [49] I. R. Hooper, J. R. Sambles, *Phys. Rev. B* **2002**, 66, 205408.
- [50] V. B. Koman, C. Santschi, O. J. F. Martin, *Anal. Chem.* **2015**, 87, 1536.
- [51] M. D. Fairchild, *Color Appearance Models*, Wiley, Chichester/West Sussex/Hoboken, NJ **2005**.
- [52] M. Bauer, *Development of Optical Thinfilm Biosensors, Dissertation, TU Wien*, **2007**.
- [53] M. Bauer, J. Haglmüller, F. Pittner, T. Schalkhammer, *J. Nanosci. Nanotechnol.* **2006**, 6, 3671.
- [54] L. Davoine, M. Schnieper, A. Barranco, F. J. Aparicio, in *Optical Sensors 2011; and Photonic Crystal Fibers V*, International Society For Optics And Photonics, Bellingham, WA **2011**, p. 807312.
- [55] H. Walter, C. Harrats, P. Müller-Buschbaum, R. Jérôme, M. Stamm, *Langmuir* **1999**, 15, 1260.
- [56] S. Arshavsky-Graham, E. Boyko, R. Salama, E. Segal, *ACS Sens.* **2020**, 5, 3058.
- [57] E. D. Palik, *Handbook of Optical Constants of Solids*, Academic Press, San Diego, CA **1998**.